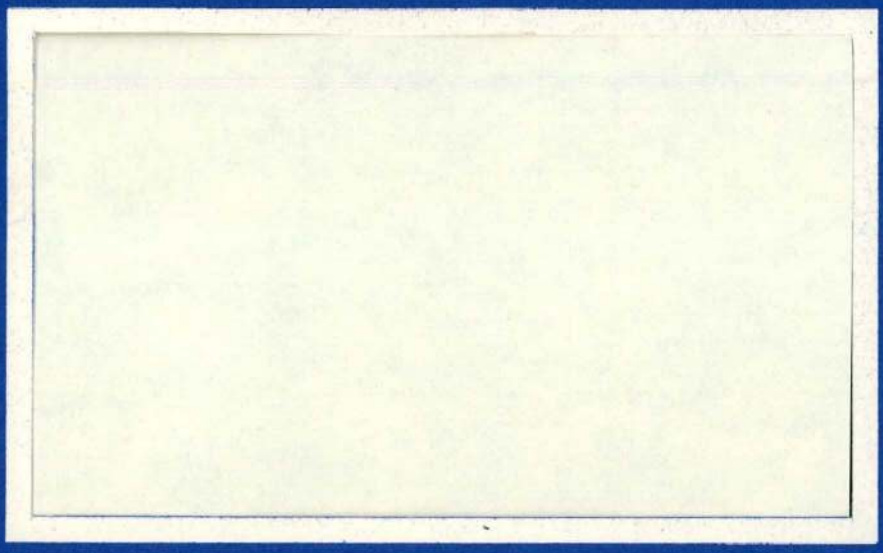

WADCO
CORPORATION
a subsidiary of Westinghouse Electric Corporation
Post Office Box 1970
Richland, Washington 99352

DISCLAIMER

HANFORD ENGINEERING DEVELOPMENT LABORATORY

Richland, Washington
operated by

WADCO CORPORATION

A Subsidiary of Westinghouse Electric Corporation
for the
United States Atomic Energy Commission Under Contract No. AT(45-1)-2170

WHAN-FR-16

UC-25
Metals, Ceramics,
and Materials

IRRADIATION PRODUCED DEFECTS IN AUSTENITIC STAINLESS STEEL

H. R. Brager
J. L. Straalsund
J. J. Holmes
J. F. Bates

December 1970

WADCO
CORPORATION
Richland, Washington 99352

UNCLASSIFIED

Printed in the United States of America
Available From
National Technical Information Service
National Bureau of Standards, U. S. Department of Commerce
Springfield, Virginia 22151
Price: Printed Copy $3.00; Microfiche $0.65

IRRADIATION PRODUCED DEFECTS IN AUSTENITIC STAINLESS STEELS

H. R. Brager, J. L. Straalsund, J. J. Holmes, and J. F. Bates

ABSTRACT

The microstructure of annealed AISI Type 304 and Type 316 stainless steels has been characterized by transmission electron microscopy as a function of fast reactor irradiation at fluence levels from 4 x 10^{21} to 7 x 10^{22} n/cm^2 (E > 0.1 MeV) and at irradiation temperatures from 370 to 700°C. Several irradiation produced defect types were found: voids, Frank faulted loops, perfect loops, dislocation networks, and precipitates. Void number density obeys a power law relationship to fluence, wherein the exponent increases with increasing temperature and has a mean value near unity. The void size is nearly independent of fluence and increases with increasing temperature. The upper limit irradiation temperature for void formation is about 650 to 700°C. The density and size of Frank faulted loops followed trends similar to those found for voids to temperatures of ~550°C where unfaulted loops, perfect loops, and dislocation networks coexist.

These experimental results do not confirm predictions of recently advanced models of void formation. The major deficiency of these models appears to be the nucleation rate. Accordingly, empirical nucleation rates were used to formulate a diffusion controlled void growth model. This model was found to closely describe experimentally determined void growth kinetics.

TABLE OF CONTENTS

LIST OF FIGURES

LIST OF TABLES

IRRADIATION PRODUCED DEFECTS IN AUSTENITIC STAINLESS STEELS

H. R. Brager, J. L. Straalsund, J. J. Holmes, J. F. Bates

INTRODUCTION

The objective of this study was to characterize the defects which develop in austenitic stainless steels during irradiation to high neutron fluence levels at temperatures between 0.38 and 0.58 T_m. Recent studies have shown that the defect state in this temperature range consists primarily of voids and interstitial Frank dislocation loops.[1,2] The volume increase and change in mechanical properties induced by void and loop formation greatly affect fast reactor design and may pose a limitation on the development of fast breeder reactors.[3,4] In order to fully understand the effects of neutron fluence and irradiation temperature upon volume and mechanical property changes, a mapping of the underlying defect concentrations and sizes is needed. Bloom and Stiegler[5] have studied the relationship between void number density and fluence at irradiation temperatures of 370 and 450°C, but as yet no complete mapping has been given.

EXPERIMENTAL PROCEDURE

Transmission electron microscopy was used to reveal the defect structure in AISI Types 304 and 316 stainless steel in the solution annealed condition. The specimens examined in this study were obtained from a number of sources. Most specimens were obtained from various components irradiated in the Experimental Breeder Reactor II (EBR-II) and included

a safety rod thimble, a control rod thimble, and an experimental subassembly thimble. Additional specimens were also taken from several EBR-II irradiation experiments. The chemical composition of all specimens was within AISI specifications for Types 304 or 316 stainless steel, Table 1. The irradiation temperature for each specimen was calculated from thermal analysis using EBR-II gamma heating values[6] and appropriate heat transfer data.

The neutron fluence was calculated by multiplying the neutron flux per MW core power by the cumulative MW exposure of the subassembly. The neutron flux was assumed to be equal to that determined by activation analysis of multiple foils irradiated during an eight day 50 MW constant power run.[7,8] The neutron flux at each specimen reactor location was interpolated from the constant reactor power flux values obtained.

Transmission electron microscopy samples were prepared from bulk samples by mechanically sectioning slabs[9] to a thickness of 0.5 mm and thinning by a two-step jet and immersion electropolishing technique.[10] The samples were examined in a Phillips 200 electron microscope operating at 100 kV using a double tilt specimen holder in a goniometer stage.

Void, loop, and precipitate densities were determined by counting the number of defects per unit area of micrograph and dividing by the foil thickness. Stereo microscopy, sliptrace analysis, and thickness contour estimates were used to determine foil thicknesses. These three methods usually produced identical foil thickness values within 100 Å for foils ranging in thickness from 500 Å to 1500 Å. Corrections were made for the intersection of voids with foil surfaces. Dislocation densities were estimated by the line intercept method.

TABLE 1

CHEMICAL ANALYSIS OF AISI TYPES 304 AND 316 SS

AISI Type	304 SS	304 SS	316 SS	316 SS
Heat No.	890810	701626	332990	65808
EBR-II Irradiation Subassembly	S.R.T.(a) C.R.T.(b)	XG05	X018	X021A X021B
C	0.07w/o	0.042	0.052	0.060
Mn	1.11	1.10	1.78	1.72
Cr	18.51	18.63	17.80	17.30
Ni	9.36	9.60	13.55	13.30
Mo	0.10	0.13	2.33	2.33
Cu	0.16	0.18	0.20	0.065
Si	0.35	0.45	0.38	0.40
P	0.006	0.30	0.012	0.012
N_2	0.029	--	0.041	0.048
B	<5 ppm	--	<5 ppm	5 ppm
S	0.015	0.013	0.020	0.007

(a) S.R.T. denotes EBR-II safety rod thimble shroud 3D1.

(b) C.R.T. denotes EBR-II control rod thimble shroud 5C3.

The size of voids and loops located totally within the foil, as revealed by stereoscopic transmission micrographs, was measured. The uncertainty in measuring the diameter of a void with a calibrated viewer was estimated to be less than 0.1 mm and corresponded to a measured variation of the void diameter of usually less than 10 Å. Each specimen was oriented in the microscope to an absorption contrast condition for delineating voids since the as-irradiated microstructure normally produced a complex, strongly diffracting image due to the large number of loops and strained lattice regions. In absorption contrast conditions, the voids appeared as light regions surrounded by a dark border. Since the thickness of the dark border is often a significant fraction of the void diameter, the total void volume determined by microscopy depends upon whether one uses the outside or inside edge of the dark border to measure the void diameter. Observations of the same voids under different contrast conditions suggest that the dark border should be considered as part of the void.

Van Landuyt et al[11] have considered the contrast effects from small voids when the crystal is oriented for the symmetrical Laue diffraction condition ($\bar{s} = 0$). According to their analysis, if there is no strain field associated with the void, the intensity of the beam passing through the foil at the void equals the intensity of a beam passing through a perfect foil which has the thickness of the original foil less the diameter of the void. This means that for $\bar{s} = 0$, as one proceeds from the matrix into the void, the transmitted intensity changes from the background intensity to a different value depending on the void size and foil thickness. The first perceptible change in intensity should indicate the surface of the void. The diameter of seven voids was measured to the

nearest 0.1 mm on 180,000X micrographs in both the symmetrical Laue condition ($\bar{s} = 0$) and in the absorption contrast condition ($\bar{s} >> 0$). Within the accuracy of the measurements, the diameter of the void for Bragg contrast condition ($\bar{s} = 0$) exactly equaled the outside diameter of the black border surrounding the light region of the void shown in absorption contrast. Therefore, the diameter of the voids was taken as the distance across the outer edges of the dark border.

RESULTS

The foils examined contained voids, Frank faulted loops, perfect loops, dislocations, and various types of precipitates, as expected from earlier work. The relationship of the defect state to fluence and temperature is described below:

VOIDS

A summary of void diameter, number density, neutron flux, neutron fluence, and irradiation temperature for the specimens examined is given in Table 2. Typical microstructure of stainless steel irradiated at specific temperatures and fast neutron fluences is shown in Figures 1 through 4. If it is assumed that the void concentration and size distribution does not depend on flux (ϕ) and time (t) but is a function only of the product ϕt (i.e., neutron fluence), the effects of irradiation void formation can be described as follows: the void concentration decreases markedly as the irradiation temperature increases and increases as the neutron fluence increases. The mean void diameter increases with increasing irradiation temperature but does not appear to change significantly with fast fluence.

TABLE 2

SUMMARY OF TRANSMISSION ELECTRON MICROSCOPY DATA

Irrad. Temp. (°C)	Fluence $n/cm^2 \times 10^{-22}$ (E>0.1 MeV)	Neutron Flux $n/cm^2\text{-sec} \times 10^{-15}$ (E>0.1 MeV)	Average Void Diameter (Å)	Void Number Density ($cc^{-1} \times 10^{-15}$)	Austenitic Stainless AISI Type	WADCO Sample Designation	Irrad. Sub-Assembly	EBR-II Irrad. Row No.
370	0.3	0.11	--	$<10^{-4}$	316	1-25-61	X018	2
370	0.4	0.11	105	1.5	304	3L	S.R.T.(a)	3
370	0.6	0.16	110	2.0	304	3K	S.R.T.	3
370	0.9	0.34	125	0.7	304	A	C.R.T.(b)	5
370	1.5	0.56	145	1.9	304	B	C.R.T.	5
375	5.6	1.52	145	5.0	304	3H	S.R.T.	3
385	3.4	1.27	150	6.5	304	C	C.R.T.	5
390	3.4	1.56	210	2.3	304	5E	XG05	4
400	5.9	1.60	200	6.0	304	3E	S.R.T.	3
420	0.9	0.49	145	1.1	316	1-21-61	X018	2
420	2.4	0.90	200	2.0	304	D	C.R.T.	5
425	2.2	0.82	210	1.7	304	E	C.R.T.	5
430	3.5	0.95	190	4.8	304	3C	S.R.T.	3
440	0.2	0.19	--	$<10^{-4}$	316	2-7	X021A	2
460	0.5	0.18	245	0.3	304	F	C.R.T.	5
525	1.9	1.03	260	0.6	316	1-18-61	X018	2
565	2.7	1.46	290	0.5	316	1-16-61	X018	2
565	0.7	1.68	315	0.05	304	37A-4-13	X067	4
595	3.0	1.62	380	0.3	304	1-14-41	X018	2
600	2.7	1.46	325	0.15	316	1-16-6CG	X018	2
700	3.0	1.81	108(c)	0.03(c)	316	1D-1	X021B	2

(a) S.R.T. denotes EBR-II safety rod thimble shroud 3D1.
(b) C.R.T. denotes EBR-II control rod thimble shroud 5C3.
(c) Probably helium bubbles.

Neg. 9288A

FIGURE 1. Structure Showing Voids in Solution-Treated Type 304 SS Irradiated at a Low Temperature, 370°C, and a Low Fast-Neutron Fluence, 4×10^{21} n/cm^2 (E > 0.1 MeV). Foil Tilted for Absorption Contrast Orientation.

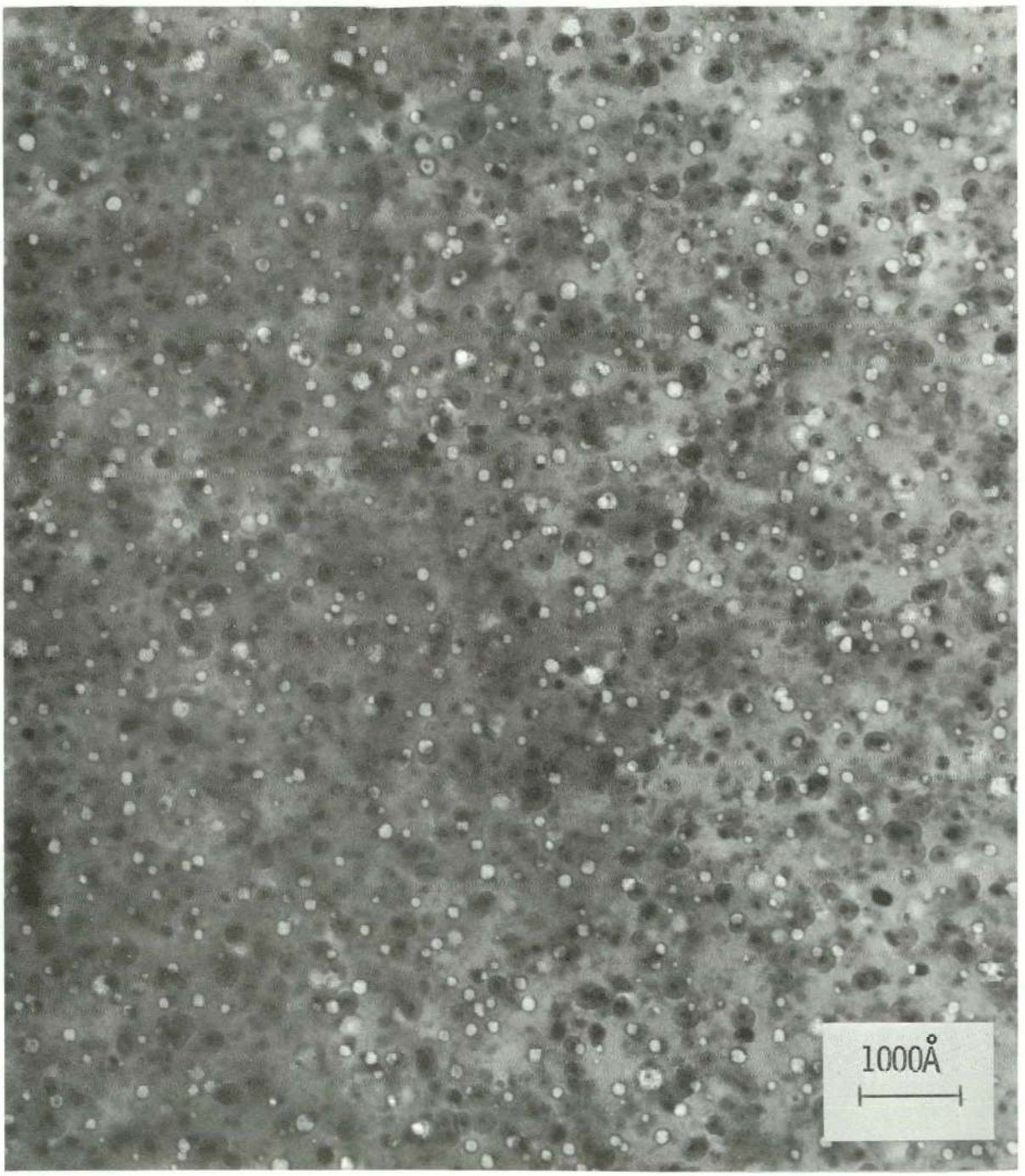

Neg. 6928A

FIGURE 2. Voids in the Same Steel Irradiated at a Low Temperature, 375°C, But a High Fast-Neutron Fluence, 5.6 x 10^{22} n/cm^2 (E > 0.1 MeV). Black Spots are Small $M_{23}C_6$ Precipitates.

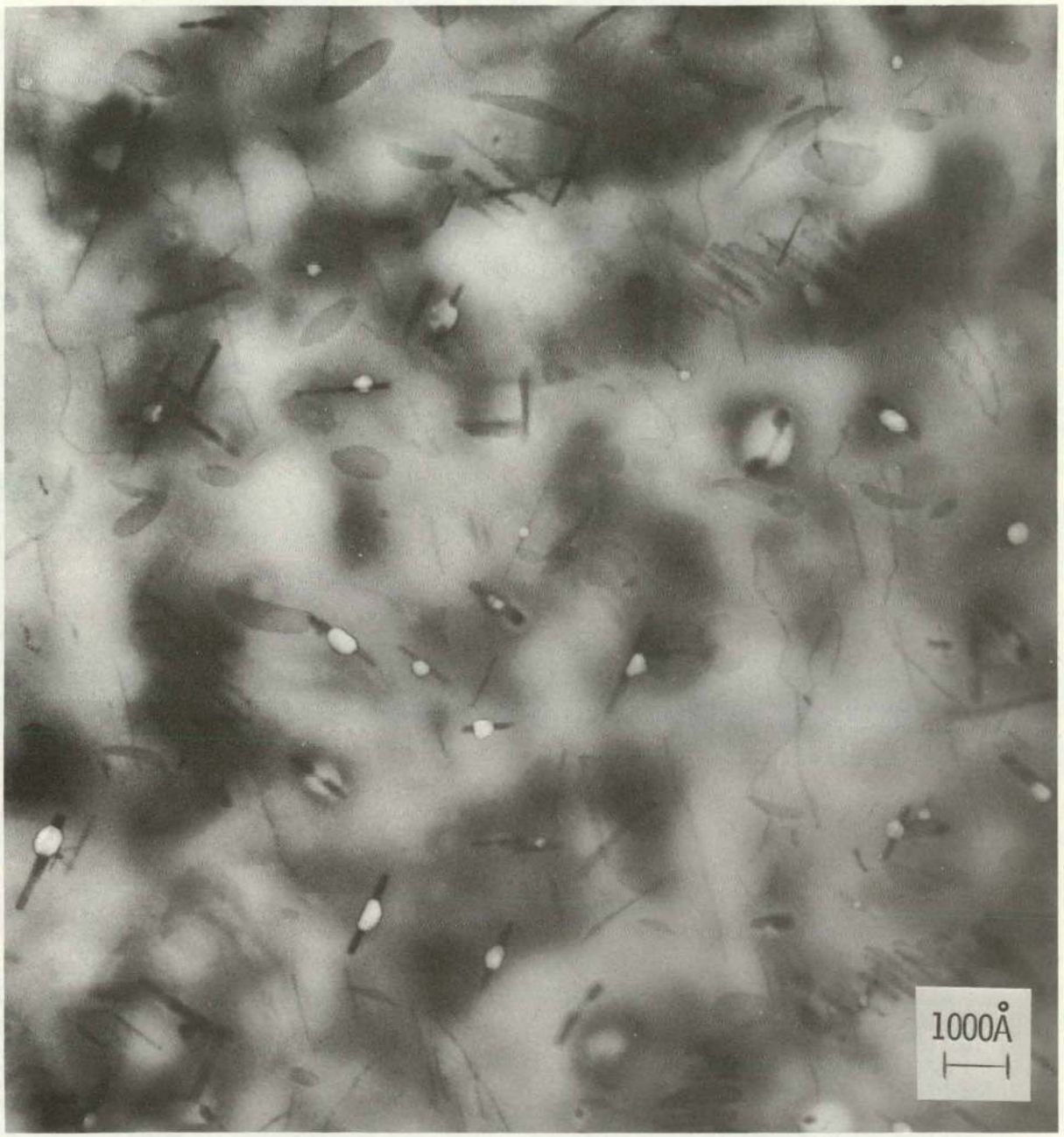

Neg. 8513A

FIGURE 3. Microstructure of the Same Steel Irradiated at a High Temperature, 565°C, But to a Low Fast Fluence, 7×10^{21} n/cm^2 ($E > 0.1$ MeV). Voids are Normally Attached to Rod Shaped Fe-Cr Sigma Precipitates. Large Frank Faulted Loops are Shown in Weak Contrast.

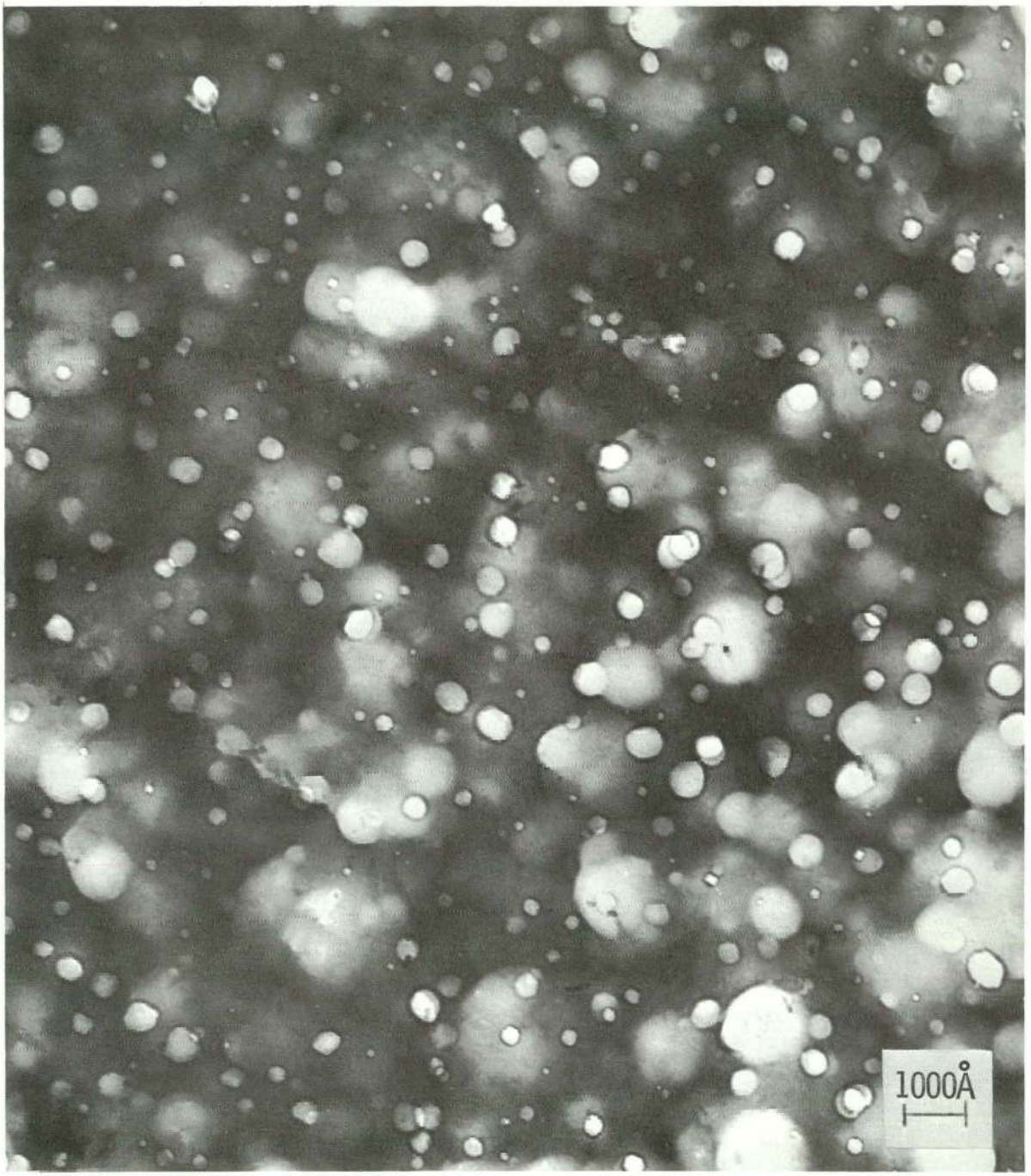

Neg. 8295C

FIGURE 4. Large Voids in Type 304 SS Irradiated at a High Temperature, 595°C, and to a High Neutron Fluence, 3×10^{22} n/cm^2 ($E > 0.1$ MeV).

Void formation in Type 304 is similar to that in Type 316 stainless steel. Some significant differences, however, do exist. Voids have not been formed ($< 10^{11}/cm^3$) in Type 316 at fluences of about 0.3×10^{22} n/cm^2, while high number densities of voids ($10^{15}/cm^3$) in Type 304 have been found at fluences of about 0.4×10^{22} n/cm^2. In addition, average void diameters appear to be somewhat smaller in Type 316 than in Type 304 stainless steel.

Empirical equations relating void size and number density to neutron fluence and irradiation temperature were developed which fit both immersion density and microscopy data. These equations were fit to data covering the irradiation temperature range from 370 to 600°C.

$$\Delta V/V = (\phi t)^{2.05^{-27/\Theta + 78/\Theta^2}} \cdot [(T - 40) \times 10^{-10}] \exp [-0.015T - 5100/T + 32.6] \quad (1)$$

$$\rho = (\phi t)^{1.60-27/\Theta + 150/\Theta^2} \exp [-0.015T + 10.253] \quad (2)$$

$$d = (\phi t)^{0.15-24/\Theta^2} \exp (7.45 - 1700/T) \quad (3)$$

$$\Delta V/V = X\rho d^3$$

where $\Delta V/V$ = % volume change

ϕt = neutron fluence ($n/cm^2 \times 10^{-22}$, [E > 0.1 MeV])

T = temperature (°K)

Θ = T-623

d = average void diameter (Å)

ρ = void number density ($number/cm^3 \times 10^{-15}$)

"X" consists of unit conversion factors and an experimentally determined geometrical conversion factor (K) which takes into account the ratio between the average of the cubed void diameter to the cube of the average void diameter (Figure 5). The above equations are only applicable at temperatures between 370 and 600°C.

It appears that the upper limit irradiation temperature for void formation in solution treated stainless steel is about 650 to 700°C. A sample of solution treated Type 316 stainless steel irradiated at 700°C to 3×10^{22} n/cm^2 (E > 0.1 MeV) contained only a low number density (3×10^{13}/cm^3) of small ($\overline{d}$ = 108 Å) cavities on grain boundaries and in the matrix. These cavities are probably helium filled bubbles.

The data used in these equations include results from the present study, Table 2, and various other sources,[1,5,12,13,14,15] Table 3. Equation (2) includes all data in Tables 2 and 3 except the low fluence Type 316 data and data from Reference (13) which appear to be much higher than the general data trends. Equation (3) includes only data from the present study because of differences in the diameter measuring techniques used among the various investigators. Typical results of Equations (1-3) are shown in Figure 6. The maximum in the void volume versus temperature curve of the irradiated steel is shown to be due to the increasing void diameter and decreasing void number density with increasing irradiation temperature.

The void size distribution appears to be a function of irradiation temperature but is relatively insensitive to neutron fluence. Void size histograms of five specimens irradiated at various conditions are shown

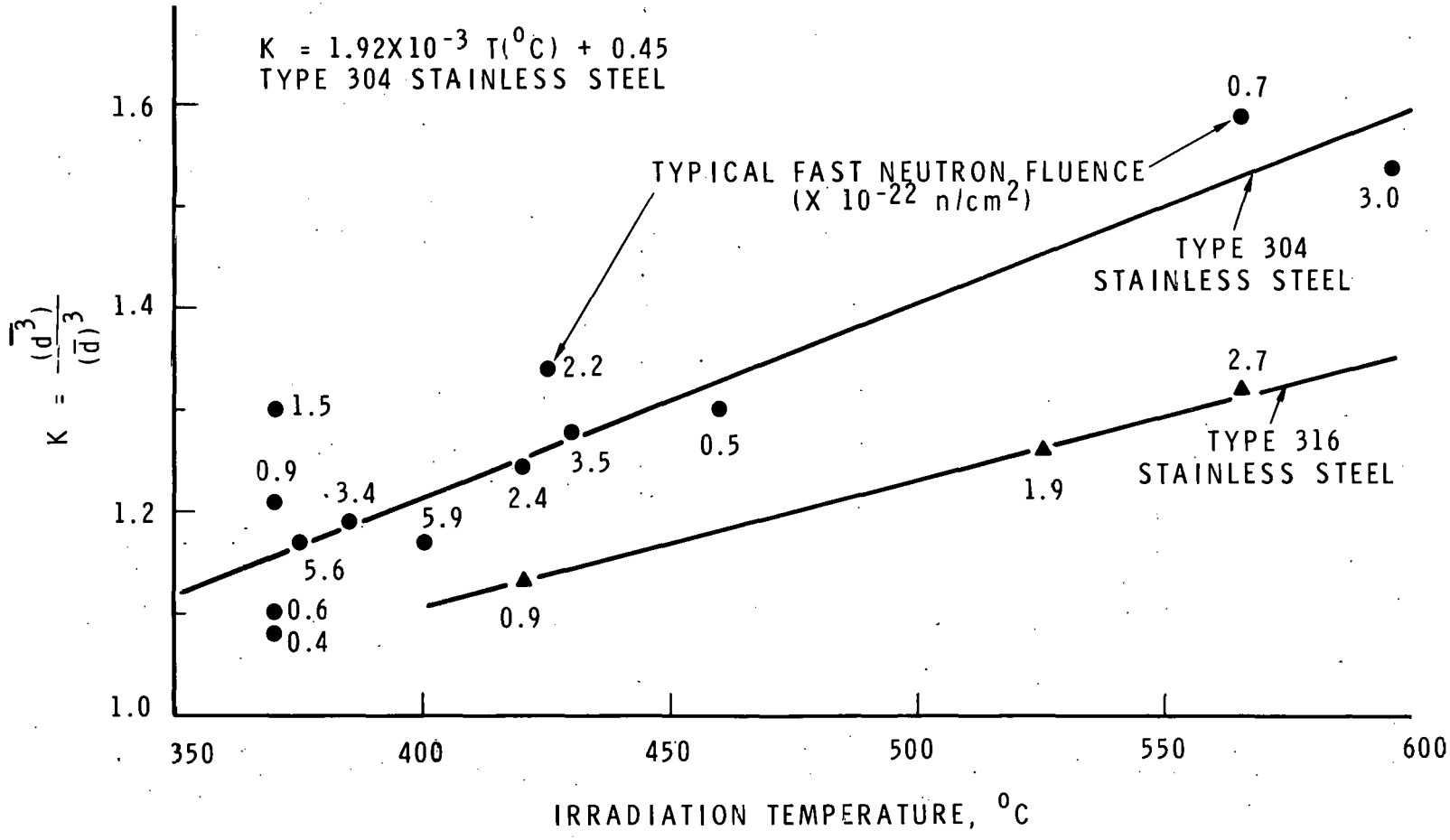

FIGURE 5. The Variation of Void Diameter Distribution Symmetry in Irradiated Austenitic SS.

TABLE 3

VOID FORMATION DATA FROM THE LITERATURE

Irrad. Temp. (°C)	Neutron Fluence (E>0.1 MeV) (n/cm^2)	Neutron Flux (n/cm^2-sec)	Average Void Diameter (Å)	Void Concentration 1/cc	Annealed AISI Type SS	Reference
450	5.2×10^{22}	(a)	135	(a)	M316	1
510	4.5×10^{22}	"	252	"		
560	3.2×10^{22}	"	258	"		
370 to 380	4.9×10^{21}	"	(a)	2.0×10^{15}	304	5
	8.0×10^{21}	"	"	2.5×10^{15}		
	1.1×10^{22}	"	"	5.0×10^{15}		
	2.3×10^{22}	"	"	7.0×10^{15}		
	5.0×10^{22}	"	"	1.0×10^{16}		
460 to 470	2.8×10^{21}	"	"	1.0×10^{14}	304	
	2.9×10^{21}	"	"	1.0×10^{14}		
	9.0×10^{21}	"	"	3.5×10^{14}		
	1.3×10^{22}	"	"	8.5×10^{14}		
	1.7×10^{22}	"	"	5.5×10^{14}		
	2.6×10^{22}	"	"	2.1×10^{14}		
375	2.4×10^{22}	"	110	(a)	304	12
410	4.5×10^{22}	"	100	"		
450	4.1×10^{22}	"	120	"		
463	3.1×10^{22}	"	200	"		
463	2.4×10^{22}	"	160	"		
660	3.0×10^{22}	"	260	1.0×10^{15}	304	13
370	0.8×10^{22}	1.4×10^{15}	80	1.4×10^{15}	304L	14
398	1.2×10^{22}	2.1×10^{15}	100	1.3×10^{15}		
430	1.4×10^{22}	2.5×10^{15}	130	1.3×10^{15}		
460	1.3×10^{22}	2.3×10^{15}	140	0.9×10^{15}		
472	0.9×10^{22}	1.6×10^{15}	160	0.4×10^{15}		
370	3.0×10^{21}	(a)	85	2.4×10^{15}	304	15

(a) not reported.

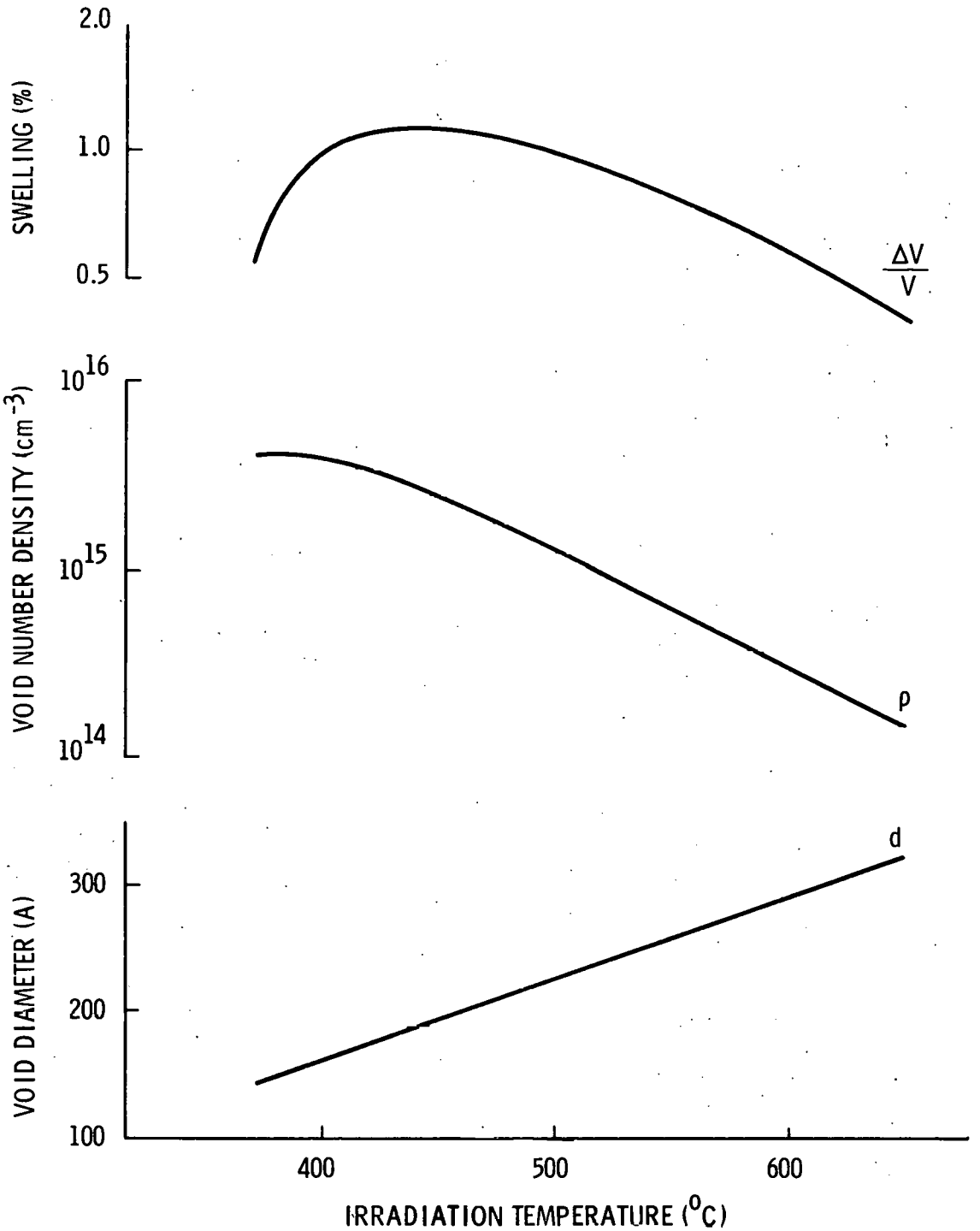

FIGURE 6. Typical Curves Based on Equations 1, 2, and 3 Showing Bulk Swelling, Void Number Density, and Void Diameter as a Function of Irradiation Temperature in Solution-Treated Type 304 and 316 SS Irradiated to 3 x 10^{22} n/cm^2 (E > 0.1 MeV).

in Figure 7. At low irradiation temperatures, a very narrow range of void diameters exists with an essentially normal distribution. As the fluence is increased an order of magnitude, the void size distribution remains normal, but the mean value increases slightly. As the irradiation temperature is increased, the normal distribution becomes skewed to larger diameters and at sufficiently high temperatures develops more than one maximum. The data are not sufficiently complete to allow the fluence and temperature dependence of the maxima to be well described.

FRANK LOOPS

The size and density of the Frank loops appear to have a fluence and temperature dependence similar to voids (Figure 8). The loop number density, at irradiation temperatures where unfaulted loops were not observed, is estimated to be an order of magnitude greater than the void density, while the average loop diameter varies from two to five times the void size. At low irradiation temperatures (370-380°C) and low fluences [4×10^{21} n/cm^2 (E > 0.1 MeV)], the microstructure consists of small faulted loops. Irradiation to high neutron fluences [6×10^{22} n/cm^2 (E > 0.1 MeV)] at low temperatures produces a high concentration of loops similar in size to those in samples irradiated to lower fluences. The structure is very complex, resulting in considerable image overlap. Loop development trends can normally only be studied at combinations of fluence and temperature where overlap is not excessive.

Under this restriction, the following trends are indicated. Loop density increases with neutron fluence and decreases with increasing temperature. The average loop size does not change appreciably with fluence but increases with irradiation temperature. The shape of the

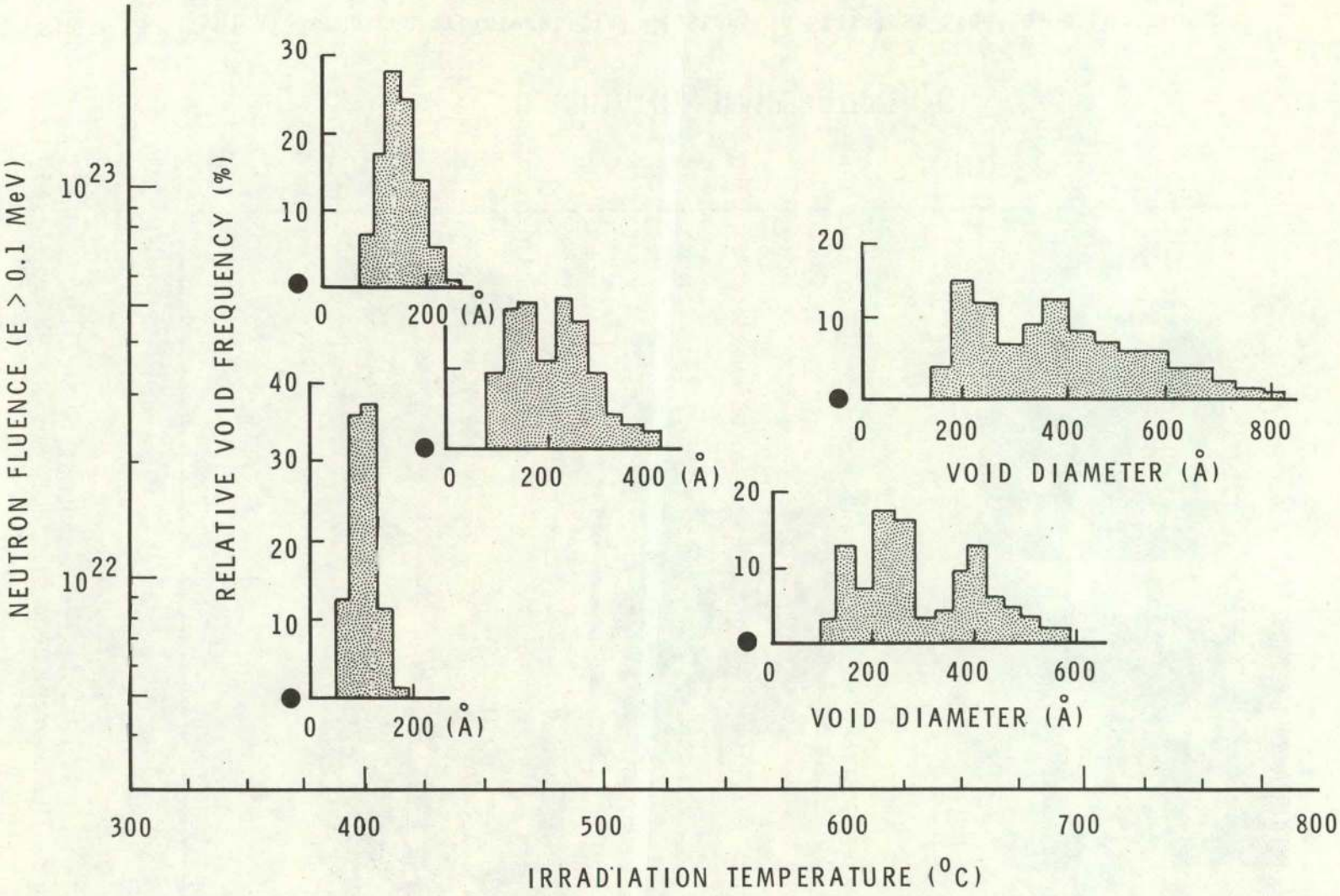

FIGURE 7. Experimentally Determined Normalized Void Size Distributions of Solution-Treated Type 304 SS as a Function of Irradiation Temperature and Fast-Neutron Fluence.

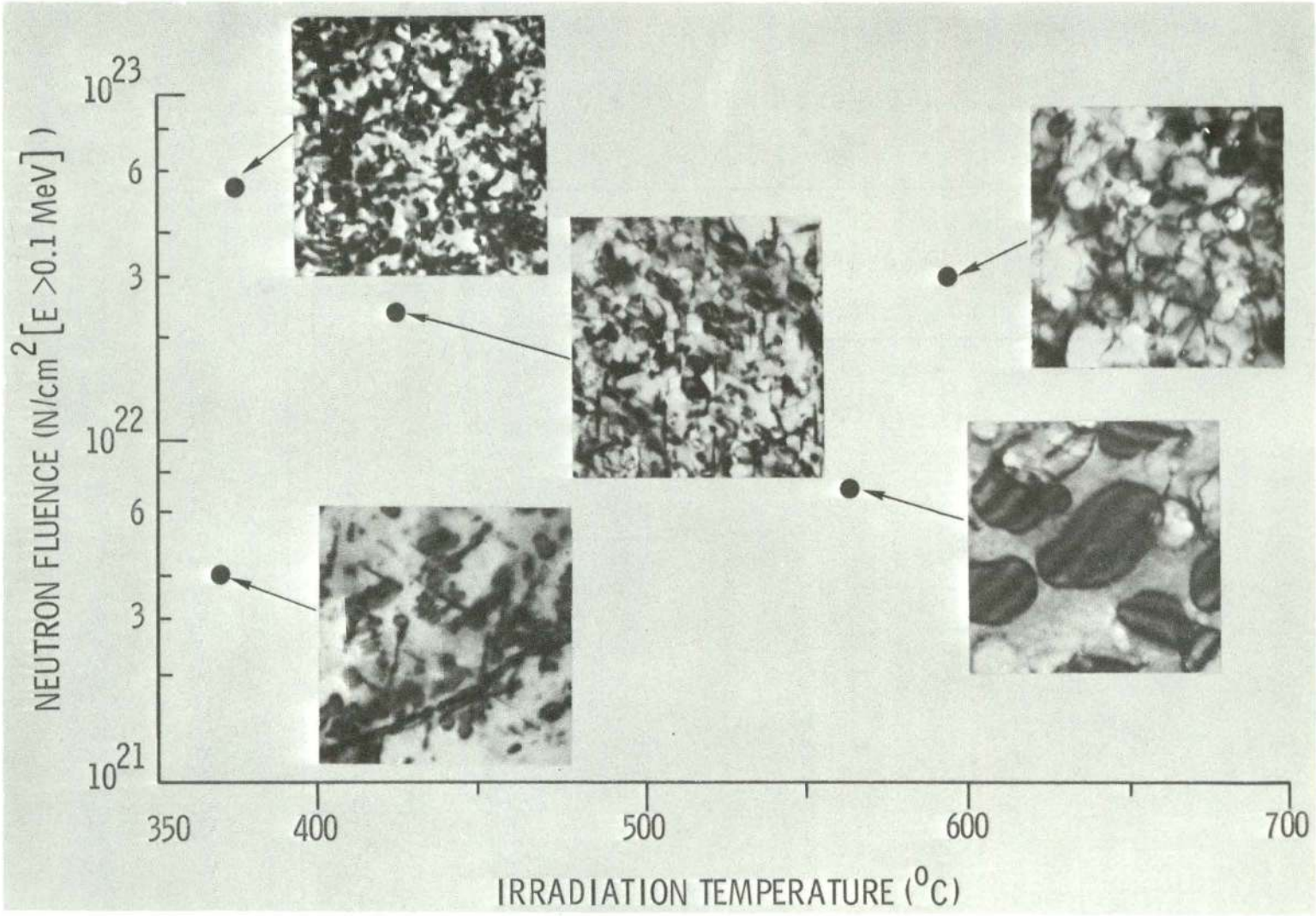

FIGURE 8. Typical Structure of Interstitial Clusters in Stainless Steel as a Function of Irradiation Temperature and Fast-Neutron Fluence.

Frank faulted loop ranges from nearly circular to very irregular. The fraction of irregular loops decreases with increasing temperature. At temperatures above 550°C, the microstructure is dominated by irregular dislocation networks and perfect loops, as shown in Figure 9. The concentration of loops and network dislocation density decrease with increasing irradiation temperature as shown in Table 4.

PRECIPITATES

The combined effects of neutron irradiation and elevated temperature also induce formation of $M_{23}C_6$ carbides and sigma phase precipitates in these steels. Specimens irradiated in the 370 to 425°C region and fluences above 1×10^{22} n/cm^2 (E > 0.1 MeV) often contain high concentrations of small (50 to 300 Å) coherent cuboidal $M_{23}C_6$ precipitates distributed uniformly throughout the matrix. Voids are not found on these coherent carbides. At higher temperatures (450 to 600°C), both larger cuboid and rod precipitate forms are found. In this region, most of the voids are normally associated with a majority of the rod shaped precipitates, although voids and rod shaped precipitates have been found independent of each other. As in the lower temperature case, voids are not associated with the cuboidal carbides at elevated temperature. The rod-like form has not been positively identified but has diffraction spots consistent with FeCr sigma phase. At the 700°C irradiation temperature, only large carbide precipitates are present.

DISCUSSION

The defect structures can be discussed in terms of irradiation temperature and fluence provided the structure is not a function of the

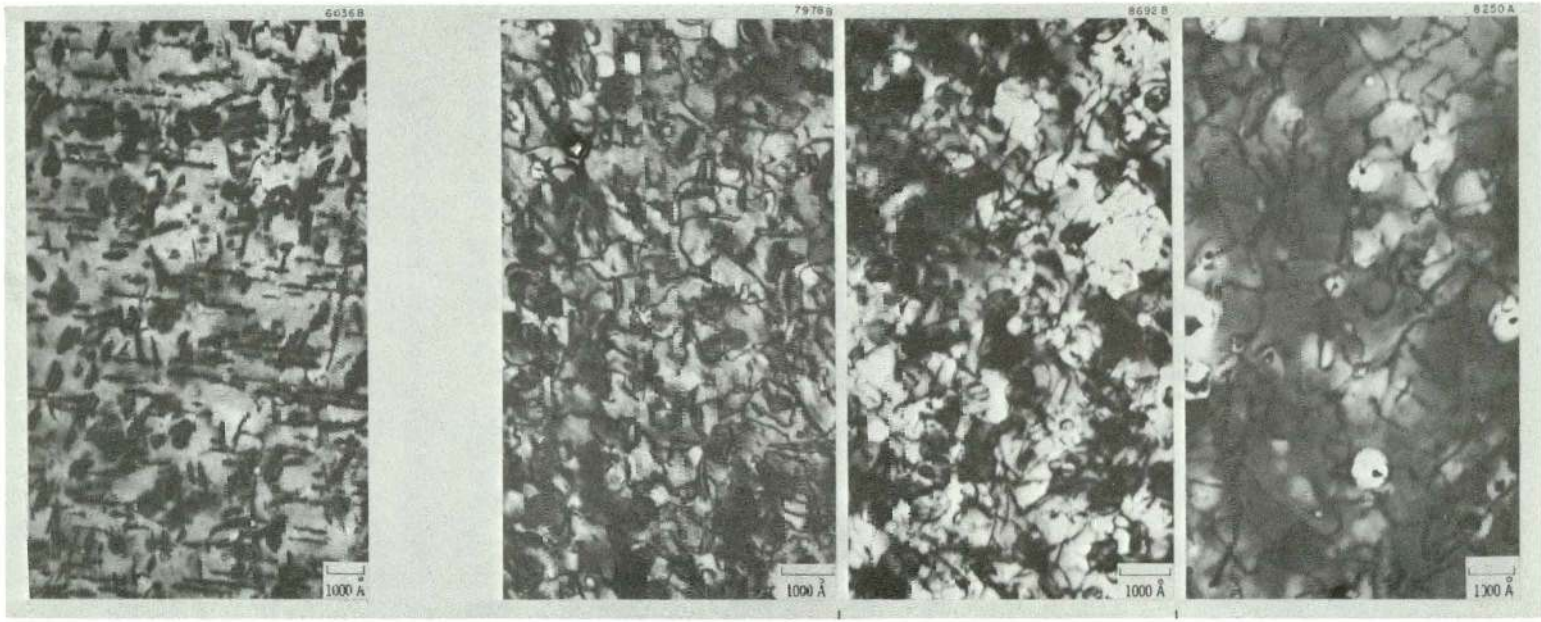

T IRRAD.=460°C	T IRRAD.=565°C	T IRRAD.=595°C	T IRRAD.=600°C
$\phi t=0.4 \times 10^{22}$	$\phi t=2.7 \times 10^{22}$	$\phi t=3.0 \times 10^{22}$	$\phi t=2.7 \times 10^{22}$
Type 304 SS	Type 316 SS	Type 304 SS	Type 316 SS
FAULTED LOOPS	DISLOCATION NETWORK FAULTED LOOPS UNFAULTED LOOPS	DISLOCATION NETWORK UNFAULTED LOOPS FAULTED LOOPS	DISLOCATION NETWORK

FIGURE 9. Micrographs Showing the Transition Between (1) Faulted Frank Loops, (2) Perfect Loops, and (3) Dislocation Networks in Types 304 and 316 SS as a Function of Irradiation Temperature.

TABLE 4

INTERSTITIAL CLUSTER STRUCTURE IN
FAST REACTOR IRRADIATED
TYPES 304 AND 316 STAINLESS STEEL

Material Type	Irrad. Temp. (°C)	Fast Neutron Fluence, n/cm^2 (E>0.1 MeV)	Faulted Loops		Dislocations and Unfaulted Loops (cm/cm^3)
			(cm^{-3})	Diameter	
304	460	0.4×10^{22}	2×10^{15}	750 Å	$< 10^9$
316	565	2.7×10^{22}	5×10^{14}	650 Å	7×10^{10}
304	595	3.0×10^{22}	6×10^{14}	350 Å	4.5×10^{10}
316	600	2.7×10^{22}	$< 10^{19}$	--	3×10^{10}

flux and time path, but their product (ϕt). While data from the present study are not sufficient to establish path independence, results from other EBR-II investigations and ion bombardment experiments can be used to clarify the situation.

Recently, Stiegler and Bloom[14] reported void size and number density results on annealed Type 304 stainless steel after EBR-II irradiation to a fluence of 0.8×10^{22} n/cm^2 at a neutron flux of 1.1×10^{15} n/cm^2-sec. These data compare favorably with the results obtained in the present study at a much lower flux of 0.16 to 0.34×10^{15} n/cm^2-sec. This agreement supports the path independence assumption of neutron fluence, but, because of the large scatter in data, a significant flux effect could easily be obscured.

Nelson and Mazey[16] and Mazey[17] have examined Type 316 stainless steel which contained various concentrations of helium and was bombarded with 20 MeV carbon ions at temperatures between 450 to 600°C. For 550°C, at damage levels reported to be similar to those obtained in fast reactor experiment, Mazey[17] reports Frank loop and void formation with sizes and concentrations similar to those found in fast reactor experiments. In this case, the loops and voids were created in a few hours compared to about 10^4 hours in reactor. This suggests that a factor greater than 10^3 increase in flux does not greatly change the defect state at equivalent fluence or damage levels. Void formation, however, was not reported at 450°C.

Laidler[18] bombarded solution treated Type 316 stainless steel, which did not contain helium, with 5 MeV Ni^{++} ions. The Ni^{++} ion bombardment

caused displacement damage in the steel calculated to be equivalent to about 3×10^{22} n/cm^2 at a rate equivalent to a neutron flux of 10^{19} n/cm^2-sec. Voids were observed for bombardment temperatures of 585°C. These voids were similar in size to voids found in steels which were neutron irradiated in the same temperature range. No voids were found for samples bombarded at 500°C or lower.

For the conditions where voids have been found, the ion bombardment studies indicate that the flux rate effect on void formation is small, particularly over the range of neutron fluxes encountered in fast reactors. However, the fluence and irradiation temperature threshold for void formation may be rate sensitive.

Recently, Laidler,[19] in the temperature range below void formation, indicated the existence of a rate effect in an ion bombarded steel. Solution treated Type 316 stainless steel was bombarded with heavy ions to the same fluence but at two orders of magnitude difference in flux. The increase in the heavy ion flux caused a decrease in "black-spot" defect cluster damage.

The effects of neutron flux on Frank loop formation are less clear than the effects on void formation. While no apparent flux effect has been found in the EBR-II experiments, accelerator studies fail to unambiguously confirm the absence of a flux effect. Mazey[17] found loop formation only at low ion dose levels; at the higher levels the loops appeared to be unfaulted and to have interacted and formed a dislocation network.

EXPERIMENTAL VOID GROWTH KINETICS

Void growth kinetics can be determined on an experimental basis by unfolding void size distributions in conjunction with experimentally

determined void nucleation rates if it is assumed that:

- Voids grow monotonically with fluence, that is, they do not undergo any shrinkage during the growth process,
- All voids nucleated at a given fluence will follow approximately the same kinetics as all other voids nucleated at that fluence,
- All voids which are above the resolvable size of transmission electron microscopy are observed and only a small fraction of voids exist below the resolution level.

The experimental void growth kinetics can be determined as illustrated schematically in Figures 10 and 11. A void size probability distribution function, Figure 10A, is generated from an experimentally determined void size histogram of a specimen irradiated to a specific fluence Φ. Typical void size histograms were previously shown in Figure 7. The void size probability function is a plot of the fraction of voids which are larger than voids having the diameter D.

The fraction of voids nucleated, which is taken as the normalized experimental void number density, as a function of neutron fluence is shown in Figure 10B. This curve is simply the density of voids calculated from Equation (2) for any fluence Φ_1, Φ_2, --- Φ_{max} divided by the void density calculated for a fluence of Φ_{max}. A tie line from any fluence level, say Φ_1, drawn vertically to the nucleation curve, then horizontally to the diameter curve, identifies the measured diameter (D_1) associated with a void which is nucleated at a fluence Φ_1 and grown during irradiation until a final fluence level of Φ is accumulated. This is equivalent to saying that the biggest void is nucleated first, the next biggest one second, and so on. Figure 10C is then constructed by plotting the

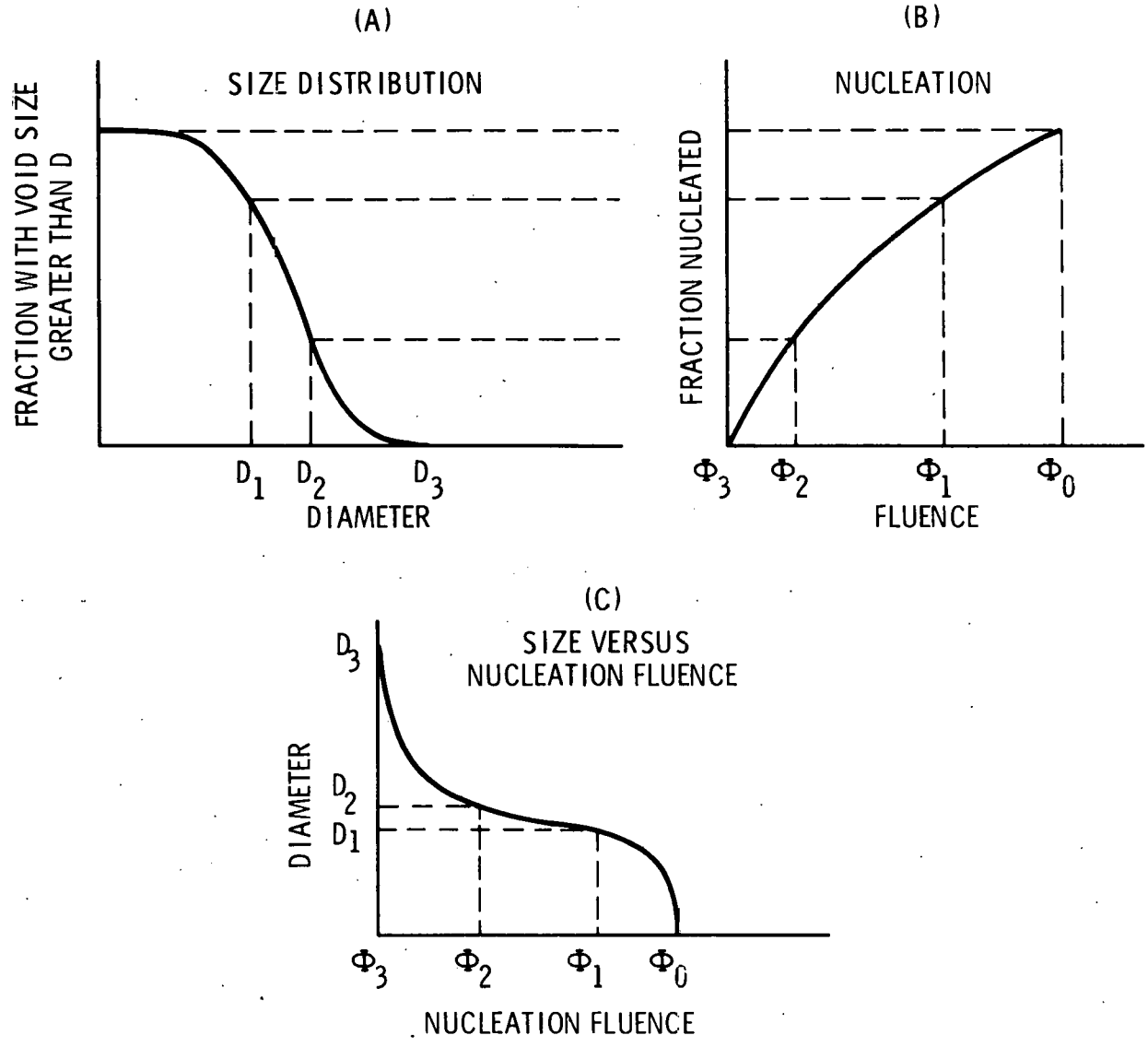

FIGURE 10. Schematic of a Void Size Probability Distribution Function and a Normalized Void Nucleation Fluence Curve Generated From Experimental Data.

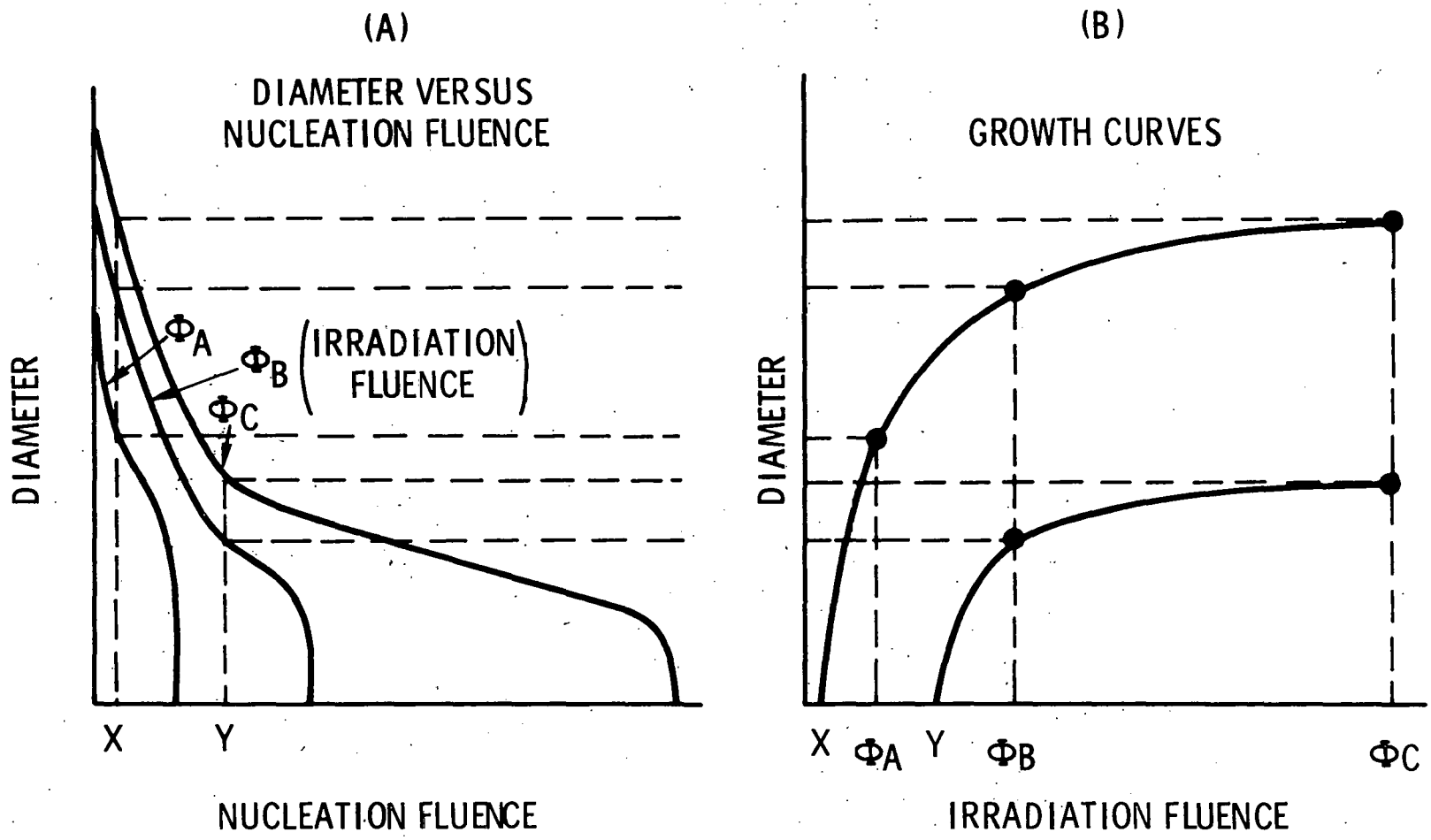

FIGURE 11. Schematic of the Determination of Experimental Void Growth Kinetics.

diameter (D) as a function of nucleation fluence (Φ).

Plots similar to Figure 10C are then constructed for various specimens irradiated to different fluences (i.e., various Φ), Figure 11A. A void growth curve may then be determined by drawing a vertical line at the nucleation fluence of interest and reading the appropriate values of diameter (D) and irradiation fluence (Φ), and then plotting the diameter (D) versus the irradiation fluence (Φ) as shown in Figure 11B.

Void growth curves are presented based on the results of five samples, all irradiated at temperatures of 370 to 380°C but over a neutron fluence from 0.4 to 5.6 x 10^{22} n/cm^2 (E > 0.1 MeV), Figure 12. The void diameter is shown to increase rapidly to about 100 Å, after which the growth rate decreases with fluence. The growth rate also appears to be a function of the fluence at which nucleation occurred. Voids nucleated at low fluences grow more rapidly than those nucleated at higher fluences. Lack of sufficient data precludes unfolding the growth kinetics at higher temperatures. The multiple peaks in the size distributions found at elevated temperatures, however, suggest that growth may proceed by somewhat different kinetics than at lower temperatures.

VOID FORMATION MECHANISMS

The importance of void formation to fast reactor technology has spurred the development of physically realistic models for void and loop nucleation and growth during irradiation. The approaches taken by Claudson et al,[20] Harkness and Li,[21,22] Bullough and Perrin,[23] and Shivley[24] all assume that void growth arises from a supersaturation of vacancies created by neutron irradiation. Growth occurs when the net rate of

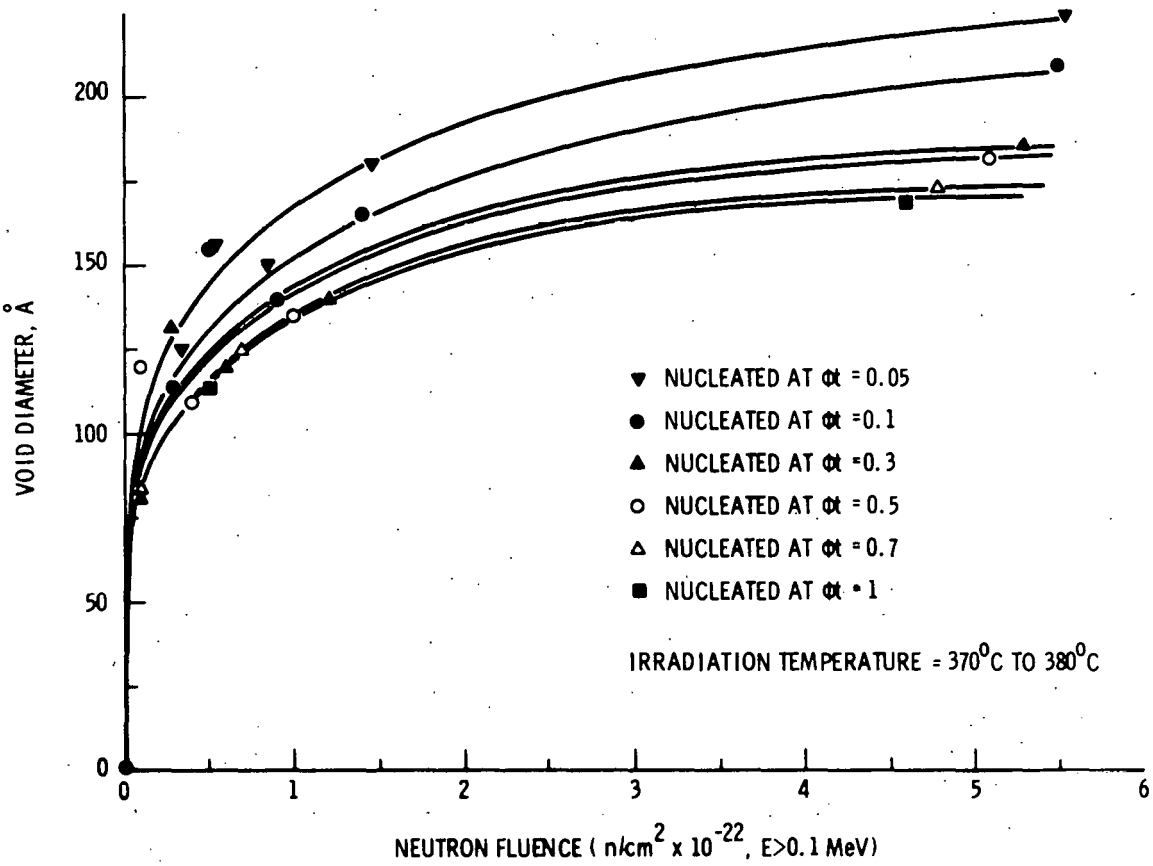

FIGURE 12. Experimental Void Growth Kinetics in Type 304 SS Irradiated at 370 to 380°C.

vacancy flow to voids exceeds the net flow rate for interstitials. Frank loops grow when the net rate of flow of interstitials exceeds the vacancy flow rate.

While general agreement exists on growth concepts, nucleation poses a difficult problem in current theory. Harkness, Li, and Tesk[22] consider nucleation behavior of voids and loops to be similar to the features of classical homogeneous nucleation. Bloom[25] demonstrated that, at low fluences, voids nucleated on dislocations and he suggested that considerable heterogeneous nucleation occurs at all fluences. Bloom and Stiegler[15] also showed that preirradiation injection of helium into stainless steel increased the number density of both voids and Frank loops. This result indicated that helium generated by fast neutron induced (n,α) reaction also affects nucleation. Other mechanisms proposed for nucleation models include growth of three dimensional vacancy clusters created in a neutron spike and heterogeneous nucleation on second phase particles.

A quantitative model for void and loop formation has been advanced by Harkness and Li.[22] This model, however, appears to be in conflict with the experimental data in terms of fluence dependency of nucleation and growth. Harkness and Li's model predicts a rapid decrease in nucleation rate with fluence. After nucleation essentially stops, voids continue to grow and dominate the volume change process. The experimental data presented here and that given by Bloom and Stiegler[5] suggest nucleation rates are nearly constant with fluence over the 370 to 600°C irradiation temperature range where voids were observed. Recently, Wolff[27] found only large voids ($d_{minimum} > 200$ Å) in annealed Type 304

stainless steel irradiated at high temperatures, 540 to 650°C, to a peak fluence of 5.4 x 10^{22} n/cm^2 (E > 0.1 MeV). The lack of small voids suggests that at this high irradiation temperature, the nucleation rate has significantly decreased or ceased during irradiation possibly due to the low vacancy supersaturation. This effect was predicted by Harkness and Li's model.

The nucleation model proposed by Harkness and Li also appears to be very sensitive to damage rate (flux). Their model predicts that accelerator experiments should produce a much higher density of smaller voids than reactor experiments, but experimentally the structures obtained by the two techniques are nearly equivalent.

Empirically determined nucleation rates may be used to compare the general features of void growth with simple growth models. Greenwood, Foreman, and Rimmer[26] and others[20-23] have considered the growth of a spherical pore in the presence of irradiation induced point defects. The defect concentrations produced during high flux neutron irradiation may be expected to be much greater than the thermal equilibrium concentrations. If it is assumed that a void has no preferential attraction for vacancies or interstitials and that internal gas pressure effects are neglected, the void growth rate may be calculated:

$$d(r^2)/dt = 2\,\Omega\,(V-I) \qquad (4)$$

where r = void radius

Ω = atomic volume

$V,I = D_V C_V,\ D_I C_I$

C_v, C_I = average vacancy and interstitial concentration in matrix

D_v, D_I = average vacancy and interstitial mobilities.

Following the treatment of Damask and Dienes,[28] point defect concentrations are considered to be maintained by a steady state dynamic balance between creation of free vacancies and interstitials, recombination of vacancies and interstitials, and migration of these defects to other sinks. This model can be expressed by the two equations:

$$\frac{dC_v}{dt} = 0 = G\phi - RVI - S_v^v V - S_v^o V \tag{5}$$

$$\frac{dC_I}{dt} = 0 = G\phi - RVI - S_I^v I - S_I^o I \tag{6}$$

where $G\phi$ is the production rate of interstitials and vacancies (the production rates have been assumed equal), S_v^v is a geometric term describing the sink efficiency of voids for vacancies, S_I^v is the geometrical term for the sink efficiency of voids for interstitials, and the S^o terms represent other sinks such as dislocations, loops, precipitates, and grain boundaries. The term RVI represents the recombination of interstitials and vacancies. Equations (5) and (6) may be solved simultaneously to yield V and I, which may in turn be substituted into Equation (4) to obtain the growth rate for a void:

$$\frac{d(r^2)}{dt} = 2\Omega\left(\frac{S'-S}{2R}\right)\left[\left(1 + \frac{4RG\phi}{S'S}\right)^{1/2} - 1\right] \tag{7}$$

where $S = S_v^v + S_v^o$

and $S' = S_I^v + S_I^o$.

If recombination is small compared to the rate of diffusion to sinks, Equation (7) may be approximated as:

$$\frac{d(r^2)}{dt} \simeq 2\Omega\left(\frac{S'-S}{S'S}\right)G\phi \qquad \left(\frac{4RG\phi}{SS'} << 1\right) \qquad (8)$$

However, if recombination predominates:

$$\frac{d(r^2)}{dt} \simeq 2\Omega(S'-S)\left(\frac{G}{RS'S}\right)^{1/2}\phi^{1/2} \qquad \left(\frac{4RG\phi}{S'S} >> 1\right) \qquad (9)$$

The predominant contributions to the sink terms S and S' are dislocation loops and voids produced during irradiation and dislocations initially present in the material. The experimental data suggest that the size and concentration of the loops and voids depend upon fluence (ϕt) rather than some other combination of flux (ϕ) and time (t). It therefore follows that S and S' are also functions of fluence. Thus if recombination is small compared to the rate of diffusion to sinks, integration of Equation (8) will yield a void radius which depends only upon fluence, in agreement with the experimental results. However, if recombination is significant, Equation (7) or (9) should be used, and it is evident that integration would yield a void radius dependent upon flux and time rather than the single fluence variable. It will be assumed, because of the apparent lack of rate dependency, that the defect concentrations are controlled predominantly by diffusion to sinks and that Equation (8) applies.

Inspection of Equation (7) shows that if all sinks have equal affinities for vacancies and interstitials (S=S') no void growth is predicted. This has been discussed in more detail by others.[17,19,23,25] Since equal amounts of vacancies and interstitials are produced during irradiation and

equal amounts are annihilated as a result of recombination, the excess vacancies that condense at voids must be balanced by an excess of interstitials condensing on other sinks such as dislocations and interstitial loops. Within this framework, there are two requirements that must be met to have void growth: 1) sinks other than voids take up the excess interstitials and 2) a driving force, or bias, tends to cause the vacancies to go to the voids and the interstitials to go to other sinks. A possible driving force, or bias,[22,26,29] is a higher sink efficiency of dislocations and loops for interstitials compared to vacancies, due to stress assisted diffusion effects as considered by Ham.[30] There is thought to be a larger strain field associated with interstitials than with vacancies, resulting in a larger elastic interaction between interstitials and dislocations than between vacancies and dislocations. Ham's analysis showed that the effect of the elastic interaction on diffusion to dislocation sinks could be represented by an increased "effective capture radius". Thus if S_v^o represents the sink term for vacancies diffusing to dislocations and dislocation loops, the term for interstitials may be approximated by:

$$S_I^o = S_v^o (1 + \varepsilon)$$

where ε represents the increased efficiency for interstitials. ε depends strongly upon the interaction energies which are very poorly known, but use of approximate interaction energies given by Damask and Dienes and the expression for capture radius given by Ham suggest that reasonable values for ε lie between 0.01 and 0.2.

The gross characteristics of the experimental void growth curves may

be shown to be consistent with diffusion controlled growth by using a simplified model which considers only voids, dislocation loops, and dislocations as sinks. The sink term for voids may be taken as:

$$S_v^v = S_I^v = 4\pi N_v \bar{r}_v$$

where N_v is the number of voids per cm^3 and $\bar{r}_v$ is the average void radius. Similarly, the sink term for interstitial loops may be approximated by the total line length associated with the loops:

$$S_v^\ell = 2\pi N_\ell r_\ell$$

$$S_I^\ell = S_v^\ell (1 + \varepsilon).$$

The sink term for dislocations is taken as the total dislocation (other than loops) line length:

$$S_v^D = \rho_D$$

$$S_I^D = S_v^D (1 + \varepsilon).$$

The relative magnitudes of S_v^ℓ and S_v^v may be compared by assuming that the number of lattice sites taken up by loops is equal to the number of lattice sites taken up by voids. With this approximation, it is possible to show that:

$$S_v^\ell \sim \frac{2 \bar{r}_v^2}{3\sqrt{3}\, \bar{r}_\ell\, a_o} S_v^v$$

where a_o is the lattice parameter. At low fluences, both $\bar{r}_\ell$ and $\bar{r}_v$ vary with fluence, but it appears reasonable to approximate the ratio S_v^ℓ/S_v^v

as a constant. At 370°C, $\bar{r}_v$ is about 50 Å and $\bar{r}_\ell$ is about 175 Å, which gives:

$$S_v^\ell \sim 5\ S_v^v.$$

If these approximations are put in Equation (8), one obtains:

$$\frac{d(r^2)}{d\phi t} = \frac{2\Omega G\ (S_v^D + S_v^\ell)\ \varepsilon}{(S_v^D + S_v^\ell + S_v^v)^2\ (1 + \varepsilon)} \sim \frac{2\Omega G\varepsilon}{(\rho_D + 24\pi\ N_v\ \bar{r}_v)} \tag{10}$$

In general, one may expect the term $N_v\ \bar{r}_v$ to vary in a complex, non-linear fashion with exposure. However, the experimental data suggest that, over a relatively wide range of fluence, the average void radius is approximately constant and the number density may be approximated as a linear function of fluence. Thus:

$$\frac{d(r^2)}{d\phi t} = \frac{2\Omega G\varepsilon}{\rho_D + B\phi t}.$$

Integration of the above equation yields

$$r^2 = \frac{2\Omega G\varepsilon}{B}\ \mathrm{Ln}\ \frac{(1 + \frac{B}{\rho_D}\phi t)}{(1 + \frac{B}{\rho_D}\phi t_n)} \tag{11}$$

where ϕt_n is the fluence at which the void was nucleated. Using the data in Table 2, and assuming an initial dislocation density of $5 \times 10^9/cm^2$, a value of about $1 \times 10^{-21}\ (n/cm^2)^{-1}$ was obtained for the ratio B/ρ_D. The best fit of Equation (11) to the experimental growth curves was obtained by choosing a value of $0.1\ (ncm)^{-1}$ for the constant $G\varepsilon$. Since reasonable values for ε appear to be between 0.01 and 0.2, this choice requires G,

the number of vacancies per cubic centimeter per unit neutron fluence surviving recombination and clustering within spikes, to be between 0.5 and 10 $(ncm)^{-1}$. This value appears to be reasonable if one considers that only a fraction of the defects produced survive recombination with the spike. The experimental growth curves are compared with curves calculated from Equation (11) in Figure 13. The general features of the calculated and experimental curves are similar, the best fit being obtained for voids nucleated early during irradiation. For voids nucleated later, the calculated curves do not have the sharp knee at 75-100 Å diameter. This knee may be due to an experimental resolution limit for observing voids having diameters significantly below 75-100 Å with the foil oriented for absorption contrast.

The void growth equation may also be used to calculate the void size distribution which, for a constant nucleation rate, may be shown to be:

$$N(r) = f(\phi t)\ r\ e^{-Br^2/2\Omega G\epsilon} \qquad (12)$$

$$\text{for } r < \frac{2\Omega G\epsilon}{B}\ \text{Ln}\ (1 + \frac{B}{\rho_D}\phi t)$$

and

$$N(r) = 0$$

$$\text{for } r > \frac{2\Omega G\epsilon}{B}\ \text{Ln}\ (1 + \frac{B}{\rho_D}\phi t).$$

A size distribution calculated from Equation (12) is compared with an experimentally determined one in Figure 14. The calculated distributions are, in general, higher than measured for the smaller void sizes, which may again reflect a decreasing resolving ability for small voids.

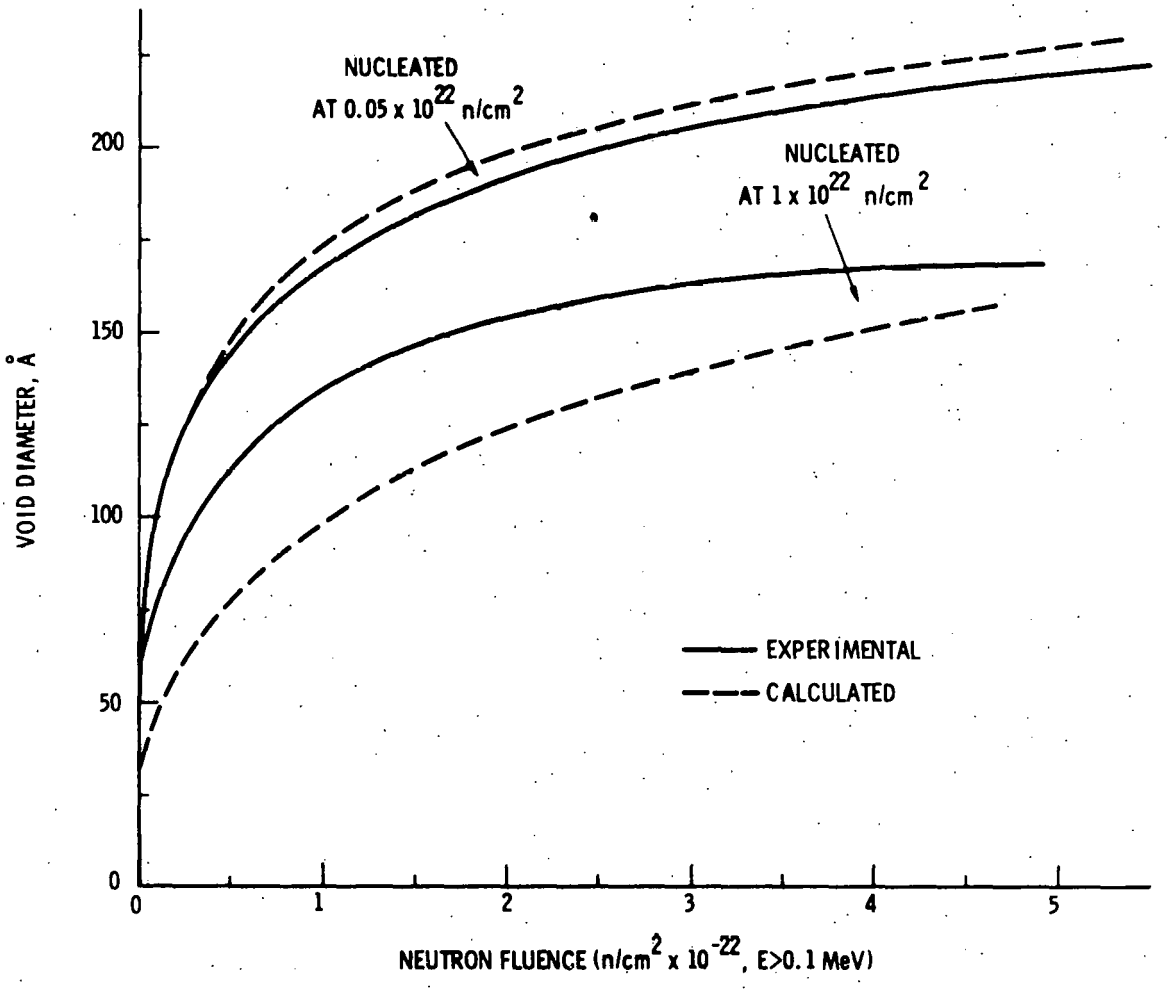

FIGURE 13. Comparison of the Experimental Void Growth Kinetics with the Theoretical Void Growth Kinetics Based on Classical Diffusion Theory.

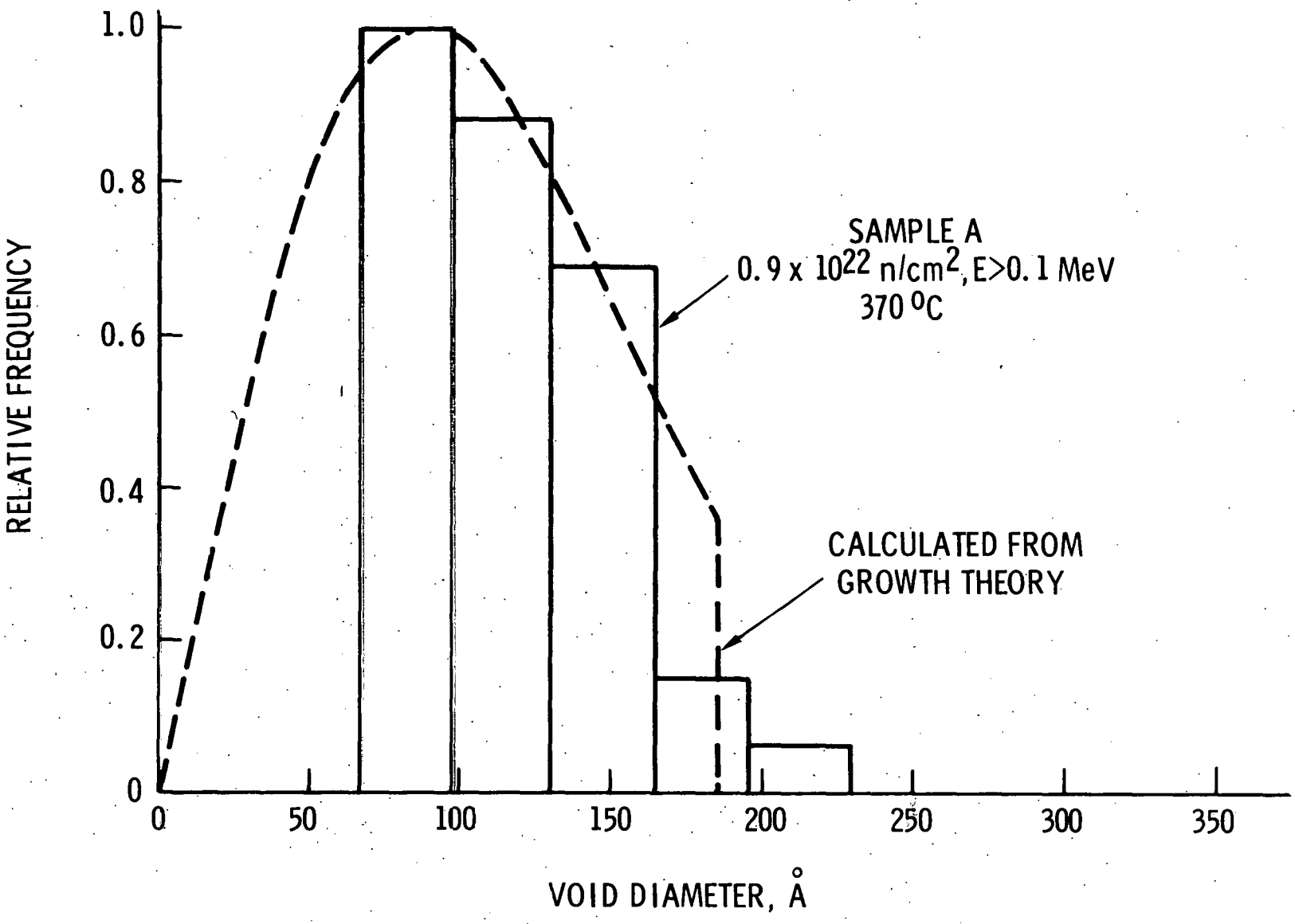

FIGURE 14. Comparison of the Experimental and Theoretical Void Size Distribution.

The void growth model employing empirical void nucleation rates and classical diffusion theory appears to closely describe the experimental void growth kinetics. However, the theory of void nucleation is not as well understood. The agreement between classical void growth theory and experimental results emphasizes the need for further investigation of the mechanisms controlling void nucleation.

CONCLUSIONS

It is concluded that:

1. The void number density follows a power law relationship to fluence with the power increasing with increasing irradiation temperature and the mean value near unity.

2. The mean void and loop size and the void size distribution are nearly independent of fluence but increase with increasing temperature. The upper limit irradiation temperature for void formation is about 650 to 700°C.

3. Void and loop formation is relatively independent of neutron flux or damage rate.

4. Frank faulted loop formation follows similar trends as void formation to about 550°C where the microstructure is dominated by an irregular dislocation network and perfect loops.

5. Void growth rates can be described in terms of classical diffusion theory using empirical nucleation rates.

ACKNOWLEDGMENTS

The authors are indebted to Mrs. M. H. Brady for preparing the electron microscopy samples and analyzing the micrographs, to Mr. R. Teats for radiometallurgical assistance, and to Mrs. H. M. Armstrong for typing the manuscript. Helpful discussions with members of the Materials Technology technical staff are gratefully acknowledged.

REFERENCES

1. C. Cawthorne and E. J. Fulton. "Voids in Irradiated Stainless Steel", Nature, Vol. 216, pp. 575-576, Nov. 1967.

2. J. J. Holmes, R. E. Robbins, J. L. Brimhall, and B. Mastel. "Elevated Temperature Irradiation Hardening in Austenitic Stainless Steel", Acta Met, Vol. 16, pp. 955-967, July 1968.

3. W. Hafele. "On the Development of Fast Breeders", The International Conference on the Constructive Uses of Atomic Energy, ANS, pp. 325-342, Washington, D. C., Nov. 1968.

4. R. J. Jackson, W. H. Sutherland, I. L. Metcalf. "Swelling and Creep Effects Upon Fast Reactor Core Structural Design", Trans. ANS, Vol. 13, No. 1, pp. 112-113, June 1970.

5. E. E. Bloom and J. O. Stiegler. "Recent Observations of Irradiation-Induced Void Formation in Austenitic Stainless Steel", Trans. ANS, Vol. 12, No. 2, pp. 589-590, Dec. 1969.

6. Guide for Irradiation Experiments in EBR-II, Revision 3. July 1969, Argonne National Laboratory, pp. 63-66 (Revised August 28, 1969).

7. W. N. McElroy, J. L. Jackson, J. A. Ulseth, and R. L. Simons. EBR-II Dosimetry Test Data Analysis (Reactor Runs 31E and 31F), BNWL-1402, Battelle-Northwest, Richland, Washington, June 1970.

8. W. N. McElroy, S. Berg, T. B. Crockett, R. J. Tuttle. "Measurements of Neutron Flux Spectra by a Multiple Foil Activation Method and Comparison with Reactor Physics Calculation and Spectrometry Measurements", Nucl. Sci. & Engr., Vol. 36, pp. 15-27, April 1969.

9. B. Mastel and H. E. Kissinger. "Wafering of Bulk Specimens for Transmission Electron Microscopy", J. Sci. Inst., Vol. 41, pp. 510-511, August 1964.

10. C. K. H. DuBose and J. O. Stiegler. "Controlled Jet Polishing of Specimens for Transmission Electron Microscopy", Rev. Sci. Inst., Vol. 38, No. 5, pp. 694-695, May 1967.

11. J. Van Landuyt, R. Gevers, and S. Amelinckx. "Diffraction Contrast from Small Voids as Observed by Electron Microscopy", Phys. Stat. Sol., Vol. 10, pp. 319-335, 1965.

12. R. Carlander, S. D. Harkness, and F. L. Yaggee. "Fast-Neutron Effects on Type-304 Stainless Steel", Nucl. Appl. & Tech., Vol. 7, pp. 67-75, Feb. 1969.

13. T. Lauritzen, A. Withop, and U. E. Wolff. "Swelling of Austenitic Stainless Steels Under Fast Neutron Irradiation at Elevated Temperatures", Nucl. Engr. & Design, Vol. 9, No 2, pp. 265-268, Feb. 1969.

14. J. O. Stiegler and E. E. Bloom. "The Effects of Large Fast-Neutron Fluences on the Structure of Stainless Steel", J. Nucl. Matl., Vol. 33, pp. 173-185, Nov. 1969.

15. E. E. Bloom and J. O. Stiegler. "The Effect of Helium on Void Formation in Irradiated Stainless Steel", J. Nucl. Matl., Vol. 36, pp. 331-334, Sept. 1970.

16. R. S. Nelson and D. J. Mazey. "Void Formation in Stainless Steel During Charged-Particle Irradiation at Elevated Temperatures", Radiation Damage in Reactor Materials, IAEA, Vol. II, pp. 157-163, Vienna, June 1969.

17. D. J. Mazey. "The Nature of Faults Formed in Association with Voids in 316 Stainless Steel During 20 MeV C^{++} Ion Bombardment", J. Nucl. Matl., Vol. 35, pp. 60-66, April 1970.

18. J. J. Laidler. "Heavy Ion Bombardment of Stainless Steel", Proc. 28th Meeting, Electron Microscopy Society of America, pp. 410-411, Houston, Texas, Oct. 1970.

19. J. J. Laidler, WADCO, Richland, Washington, private communication, 1970.

20. T. T. Claudson, J. J. Holmes, J. L. Straalsund, and H. R. Brager. "Fast-Reactor Radiation-Induced Changes in Cladding and Structural Materials", Radiation Damage in Reactor Materials, IAEA, Vol. II, pp. 165-187, Vienna, June 1969.

21. S. D. Harkness and Che-Yu Li. "A Model for Void Formation in Metals Irradiated in a Fast-Neutron Environment", Radiation Damage in Reactor Materials, IAEA, Vol. II, pp. 189-214, Vienna, June 1969.

22. S. D. Harkness, J. A. Tesk, and Che-Yu Li. "An Analysis of Fast Neutron Effects on Void Formation and Creep in Metals", Nucl. Appl. & Tech., Vol. 9, pp. 24-30, July 1970.

23. R. Bullough and R. C. Perrin. "Growth, Stability, and Interactions of Voids and Gas Bubbles in Solids", Radiation Damage in Reactor Materials, IAEA, Vol. II, pp. 233-251, Vienna, June 1969.

24. J. H. Shively. Radiation Damage in Reactor Materials, IAEA, Vol. II, pp. 253-255, Vienna, June 1969.

25. E. E. Bloom. "An Investigation of Fast Neutron Radiation Damage in an Austenitic Stainless Steel", ORNL-4580, June 1970.

26. G. W. Greenwood, A. J. E. Foreman, and D. E. Rimmer. "The Role of Vacancies and Dislocations in the Nucleation and Growth of Gas Bubbles in Irradiated Fissile Materials", J. Nucl. Matl., Vol. 1, No. 4, pp. 305-324, Dec. 1959.

27. D. W. Sandusky and U. E. Wolff. "Irradiation Temperature Dependence of Void Formation in Type 304 Stainless Steel", J. Nucl. Matl., to be published.

28. A. C. Damask and G. J. Dienes. Point Defects in Metals, Gordon and Breach Science Publishers, New York, 1963.

29. T. T. Claudson, R. W. Barker, and R. L. Fish. "The Effects on Fast Flux Irradiation on the Mechanical Properties and Dimensional Stability of Stainless Steel", Nucl. Appl. & Tech., Vol. 9, pp. 10-23, July 1970.

30. F. S. Ham. "Stress-Assisted Precipitation on Dislocations", J. Appl. Physics, Vol. 30, No. 6, pp. 915-926, June 1959.

DISTRIBUTION

No. of Copies

OFFSITE

1 AEC Chicago Patent Group
- G. H. Lee, Chief

29 AEC Division of Reactor Development & Technology
- Director, RDT
- Asst Dir for Nuclear Safety
- Analysis & Evaluation Br, RDT:NS
- Asst Dir for Plant Engr, RDT
- Facilities Br, RDT:PE
- Components Br, RDT:PE
- Instrumentation & Control Br, RDT:PE
- Liquid Metal Systems Br, RDT:PE
- Asst Dir for Program Analysis, RDT
- Asst Dir for Project Mgmt, RDT
- Liquid Metals Projects Br, RDT:PM
- FFTF Project Manager, RDT:RE
- Asst Dir for Reactor Engr, RDT
- Control Mechanisms Br, RDT:RE
- Core Design Br, RDT:RE
- Fuel Engineering Br, RDT:RE
  - A. C. Millunzi
  - C. E. Weber
- Fuel Handling Br, RDT:RE
- Reactor Vessels Br, RDT:RE
- Coolant Chemistry Br, RDT:RT
- Fuel Recycle Br, RDT:RT
- Fuels & Materials Br, RDT:RT
  - T. C. Reuther, Jr.
  - K. M. Zwilski
- Reactor Physics Br, RDT:RE
- Special Technology Br, RDT:RT
- Asst Dir for Engr Standards, RDT
- LMFBR Program Manager, RDT:PM

210 AEC Division of Technical Information Extension

1 AEC Idaho Operations Office
Nuclear Technology Division
- C. W. Bills, Director

1 AEC San Francisco Operations Office
Director, Reactor Division

No. of Copies	
7	AEC Site Representatives Argonne National Laboratory - CH Argonne National Laboratory - ID Atomics International General Electric Company Westinghouse Electric Corporation
7	Argonne National Laboratory R. Carlander — LMFBR Program Office S. D. Harkness — P. G. Shewman R. A. Jaross — N. J. Swanson C. Y. Li
1	Atomic Power Development Association Document Librarian
11	Atomics International L. Bernath — D. W. Keefer FFTF Program Office — H. Pearlman K. Garr — J. H. Shivley D. Kramer
2	Babcock & Wilcox Company Atomic Energy Division S. H. Esleeck G. B. Garton
2	Battelle Memorial Institute M. Kangilaski J. S. Perrin
5	Bechtel Corporation F. A. Comprelli J. J. Teachnor
1	Bettis Atomic Power Lab F. A. Nichols
1	Combustion Engineering 1000 MWe Follow-On Study W. P. Staker, Project Manager

No. of Copies	
1	Combustion Engineering Mrs. Nell Holder, Librarian
5	General Electric Company Advanced Products Operation Karl Cohen (3)
4	General Electric Company Breeder Reactor Dev. Oper. 310 DeGuigne Drive Sunnyvale, CA 93806 W. K. Appleby, D. W. Sandusky H. Busboom, C. N. Spalaris
1	General Electric Company Nucleonics Laboratory P. O. Box 846 Pleasanton, CA 94566 Dr. H. W. Alter, Mgr.
2	Gulf General Atomic Inc. General Atomic Division D. Coburn
1	Idaho Nuclear Corporation J. A. Buckham
1	Liquid Metal Engineering Center R. W. Dickinson
2	Liquid Metal Information Center A. E. Miller
1	Naval Research Laboratory F. A. Smidt, Jr.
1	Massachusetts Institute of Technology A. L. Bement, Jr.

No. of Copies	
1	North American Rockwell Corporation Science Center 1049 Camino Dos Rios Thousand Oaks, CA 91360 H. W. Wiedersick
1	North Carolina State University J. R. Beeler
4	Oak Ridge National Laboratory E. E. Bloom W. O. Harms J. O. Stiegler
1	Stanford University Nuclear Division Division of Mechanical Engineering R. Sher
1	United Nuclear Corporation Research and Engineering Center R. F. DeAngelis
1	University of Cincinnati J. Moteff
1	Vallecitos Nuclear Center Vallecitos Road Pleasanton, CA 94566 U. E. Wolff
13	Westinghouse Electric Corporation Atomic Power Division Advanced Reactor Systems A. Biancheria A. Boltax D. C. Spencer K. C. Thomas
2	Westinghouse Research Laboratory Pittsburgh, PA R. T. Begley R. Stickler

No. of Copies

ONSITE

1 AEC Chicago Patent Group

R. K. Sharp (Richland)

4 AEC RDT Site Representatives

P. G. Holsted
J. H. Sako

1 AEC Richland Operations Office

J. M. Shivley

8 Battelle-Northwest

BNW Technical Information Files (5)
J. L. Brimhall
H. E. Kissinger
G. L. Kulcinski

1 Bechtel Corporation

W. A. Smith (Richland)

2 RDT Asst Dir for Pacific Northwest Programs

T. A. Nemzek

1 WADCO Representative

R. M. Fleischman

111 WADCO Corporation

R. W. Barker
J. F. Bates (10)
T. K. Bierlein
L. D. Blackburn
W. F. Brehm
H. R. Brager (50)
T. T. Claudson
W. V. Cummings
R. E. Dahl
D. G. Doran
W. H. Esselman
E. A. Evans
R. L. Fish
E. R. Gilbert
S. M. Gill
G. L. Guthrie
J. E. Hanson
L. A. Hartcorn
B. R. Hayward
J. J. Holmes (10)
C. W. Hunter
J. E. Irvin
J. J. Laidler
R. D. Leggett
R. J. Leitz
A. J. Lovell
B. Mastel
W. N. McElroy
R. A. Moen
D. P. O'Keefe
D. G. Ott
M. M. Paxton
W. F. Sheely
F. R. Shober
J. L. Straalsund (10)
J. C. Tobin
A. L. Ward
J. A. Williams
B. Wolfe
H. H. Yoshikawa
WADCO Document Control (15)
WADCO Tech Pubs (2)